Supporting Information

Rational Molecular Design of Electrocatalysts Based on Single-Atom Modified Covalent Organic Frameworks for Efficient Oxygen Reduction Reaction

Kazuyuki Iwase,[†,‡] Shuji Nakanishi[‡,§] Masaru Miyayama[†] and Kazuhide Kamiya,[,‡,§,‖]*

†Department of Applied Chemistry, The University of Tokyo, 7-3-1 Hongo, Bunkyo-ku, Tokyo 113-8656, Japan.
‡Research Center for Solar Energy Chemistry, Osaka University, 1-3 Machikane-yama, Toyonaka, Osaka 560-8531, Japan.
§ Graduate School of Engineering Science, Osaka University, 1-3 Machikaneyama, Toyonaka, Osaka 560-8531, Japan.
‖ Japan Science and Technology Agency (JST) PRESTO, 4-1-8 Honcho, Kawaguchi, Saitama 332-0012, Japan.

*E-mail for K.K.: kamiya@chem.es.osaka-u.ac.jp.

Supporting Tables and Figures

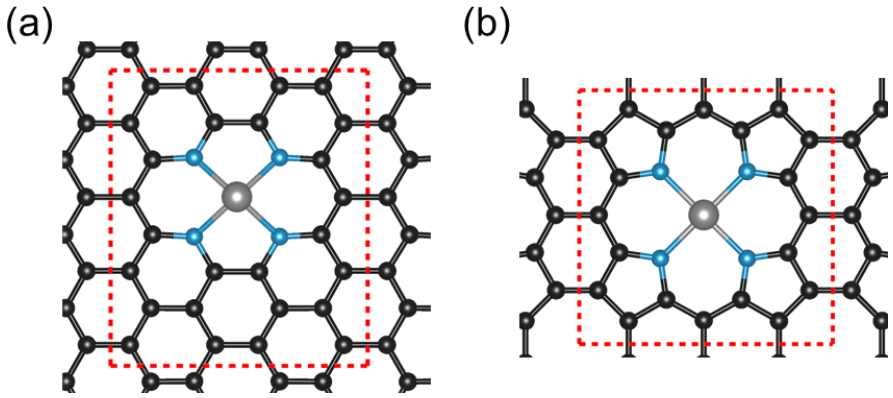

Figure S1. Model structures of graphitic materials with metal centers coordinated by 4 N atoms, which are designed by following previous reports by F. Calle-Vallejo et al.[1,2] (a) Graphitic material type a and (b) Graphitic materials type b. Gray; transition metal atoms (M), black: C, blue: N and red: O. Red dotted lines represent the unit cell for each structure model.

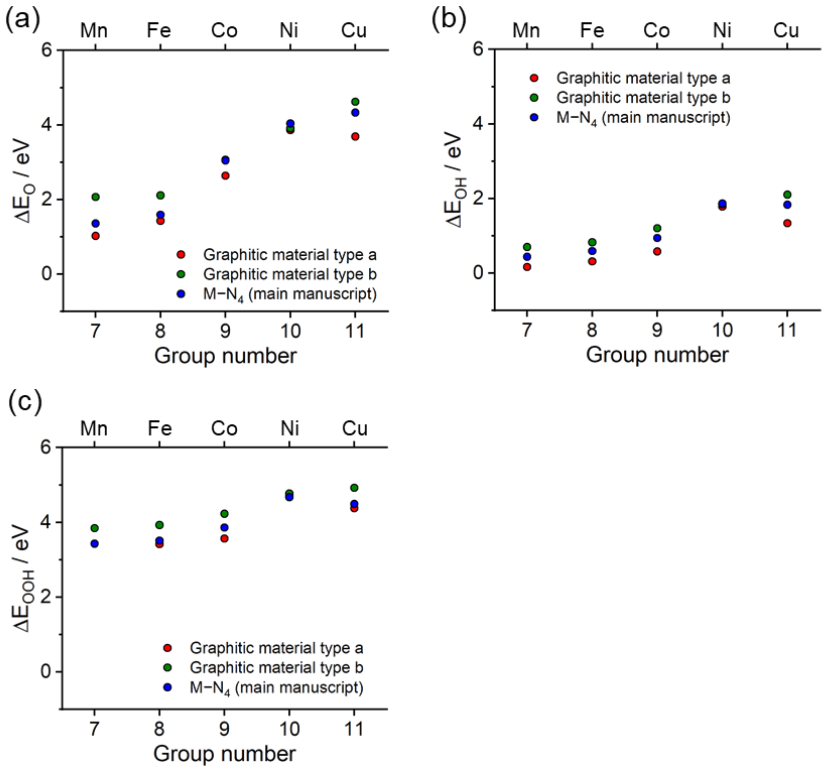

Figure S2. Adsorption energies of ORR intermediates (ΔE_{ads}) to metal centers ((a) O, (b) OH and (c) OOH) using graphitic material models shown in Figure S1. Red symbols: graphitic materials type a, green symbols: graphitic materials type b. Blue symbols represent the replotted value of $M-N_4$ in the main manuscript for the comparison.

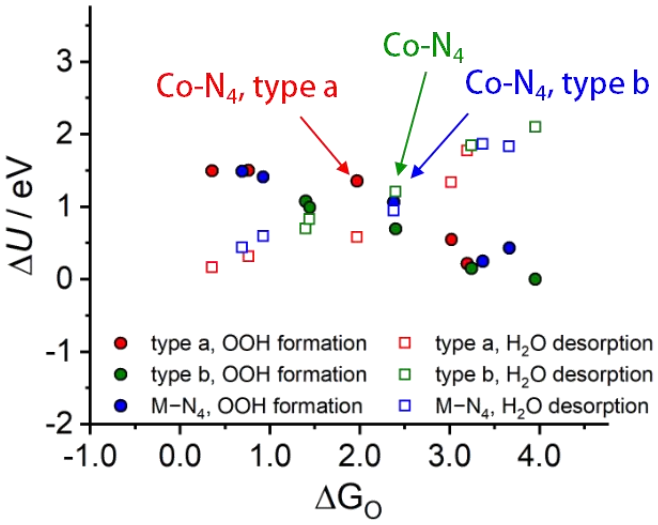

Figure S3. Potential plots for the limiting steps of the ORR against the ΔG_O of metal-nitrogen doped graphitic materials shown in Figure S1. The y axis is calculated based on the equation in the Computational details section. Potentials for $M-N_4$ in the main manuscript are re-plotted for the comparison.

Table S1. ZPE, TS and $E_{solvation}$ used in this study to calculate formation energy (ΔG) of ORR intermediates. The value is taken from previous reports.[3–6]

Species (phase)	ZPE	TS	$E_{solvation}$
H_2(g)	0.27[a]	0.404 [a]	- [a]
H_2O(l)	0.574 [a]	0.583 [a]	-0.087 [a]
OH*	0.332 [a]	- [a]	-0.38[c]
OOH*	0.428 [a]	- [a]	-0.47[c]
O*	0.07[b]	- [b]	-0.70[c]
O_2	0.08[c]	-	-0.41[c]

a: Ref. 3, b: Ref. 4, c: Ref. 5,6.

Table S2. Stabilization energies ($E_{stabilize}$) of metal ions for $M{-}N_2$, $M{-}N_3$, $M{-}N_4$. Metal atoms on pristine graphene and bulk metals are calculated as references. Every value in this table is described in eV unit.

	$M{-}N_2$	$M{-}N_3$	$M{-}N_4$	M on pristine Graphene	M on bulk metals
Mn	−1.81	−2.59	−8.72	−0.10	n.c.[a]
Fe	−2.03	−2.96	−9.20	−0.79	−4.88
Co	−2.72	−3.25	−9.29	−0.96	n.c.[a]
Ni	−2.69	−3.17	−8.86	−1.18	n.c.[a]
Cu	−1.84	−2.31	−7.05	−0.06	−4.58

n.c.[a] : not calculated

Note: These values are similar with those in the previous reports about low-coordination metal sites (CN=2 or 3).[7–9] As predicted, lower-coordination metals became more unstable. Some metal centers in M−COFs are less stable than those on bulk metals. This result means that single metal sites in M−COFs are metastable. However, metal atoms in COFs with low CN (CN=2, 3) are obviously more stable than metal atoms embedded on pristine graphene as references. Considering these $E_{stabilize}$ values, M−COF are stable enough to employ these single-atom-modified COFs as the model structure for the calculation.

Table S3. Effect of the addition of Hubbard correction (*U*) to the 3d electrons. ΔE_O values in the main manuscript are also shown as references.

	ΔE_O by GGA + *U* method			ΔE_O in the main manuscript		
	M−N_2	M−N_3	M−N_4	M−N_2	M−N_3	M−N_4
Co	1.45	1.69	4.32	0.16	0.81	3.05
Cu	1.93	2.54	4.51	1.36	1.90	4.33

Note: GGA + *U* with a *U* value of 5 eV was applied to 3d electron of metal centers. 5 eV was chosen from previous study which reported GGA + *U* calculation results on SAC with Cu−N_3 like local structure.[10] The same tendency of ΔE_O, CN and d electron number dependence, was observed even in GGA + *U* method. However, the absolute values show certain difference from the results obtained in the method without + *U* for both M−COFs. This result indicates that further analysis by using various kind of base function and/or DFT method can be a future work of this study.

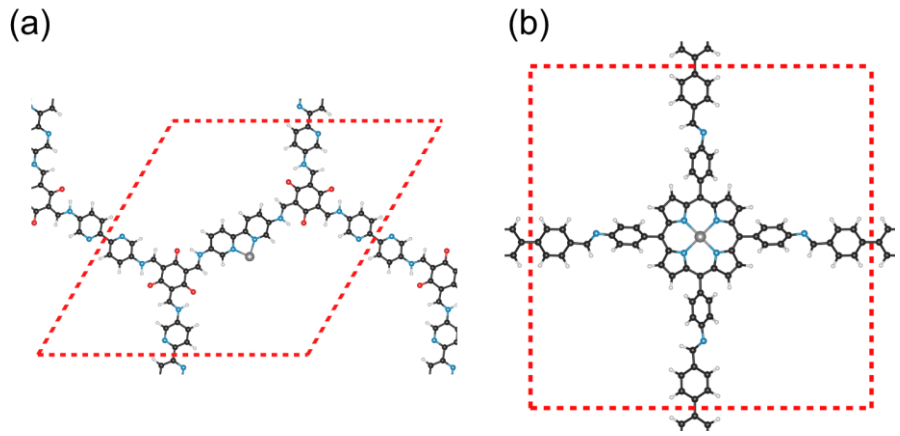

Figure S4. Model structure employed in this study. (a) Bipyridine-type unit cells similar molecular structure to M–N_2 in the main manuscript based on the reported COF by Banerjee et al.[11] (named M–N_2–2) and (b) porphyrin-type unit cell similar molecular structure to M–N_4 based on the reported COF by Yaghi et al.[12] (named M–N_4–2). Both images display the structures after structural optimization. Gray: transition metal atoms (M), black: C, white: H, blue: N, red: O. The red dotted lines represent the unit cell for each structural model.

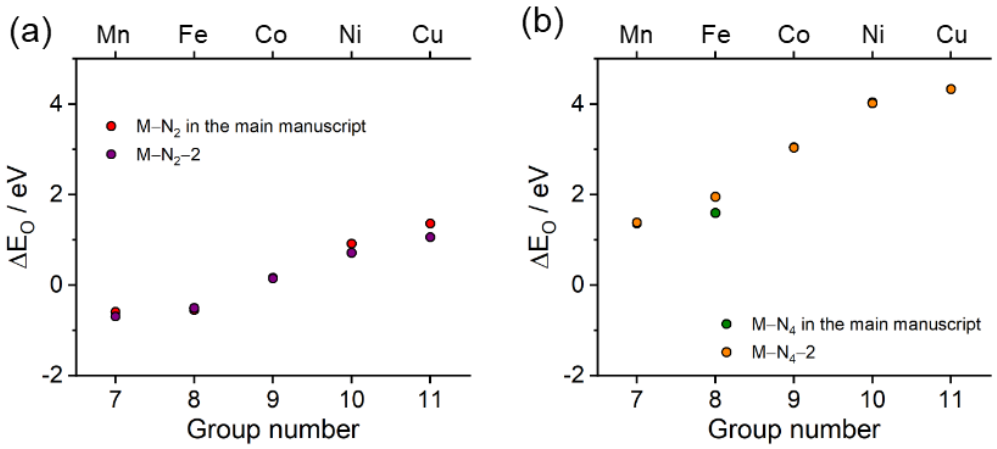

Figure S5. Adsorption energies of O atom (ΔE_{ads}) to metal centers using previous reported COF structure shown in Figure S4. ΔE_O of M−COFs for (a) M−N_2−2, and (b) M−N_4−2. For both graphs, ΔE_O value of M−N_2 or M−N_4 in the main manuscript are also re-plotted for the comparison.

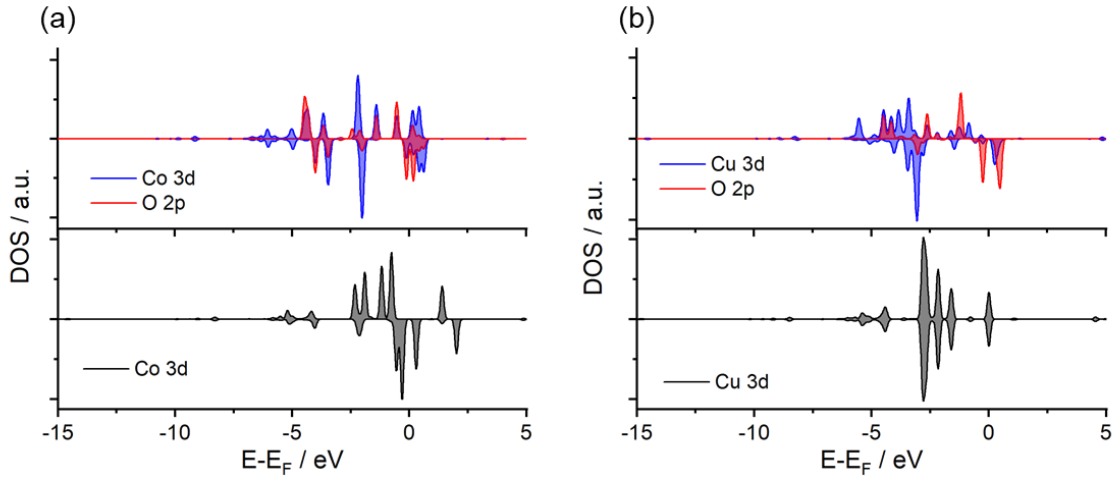

Figure S6. Representative PDOS of (a) Co−N_4 and (b) Cu−N_4. For both figures, upper parts (colored lines) represent the PDOS of M−N_4 with O atoms (*O) and bottom parts (black lines) represent M−N_4 without adsorbates. Blue lines and red lines represent the d orbitals of metal atoms in M−N_4 and p orbitals of O atoms of O adsorbed M−N_4, respectively.

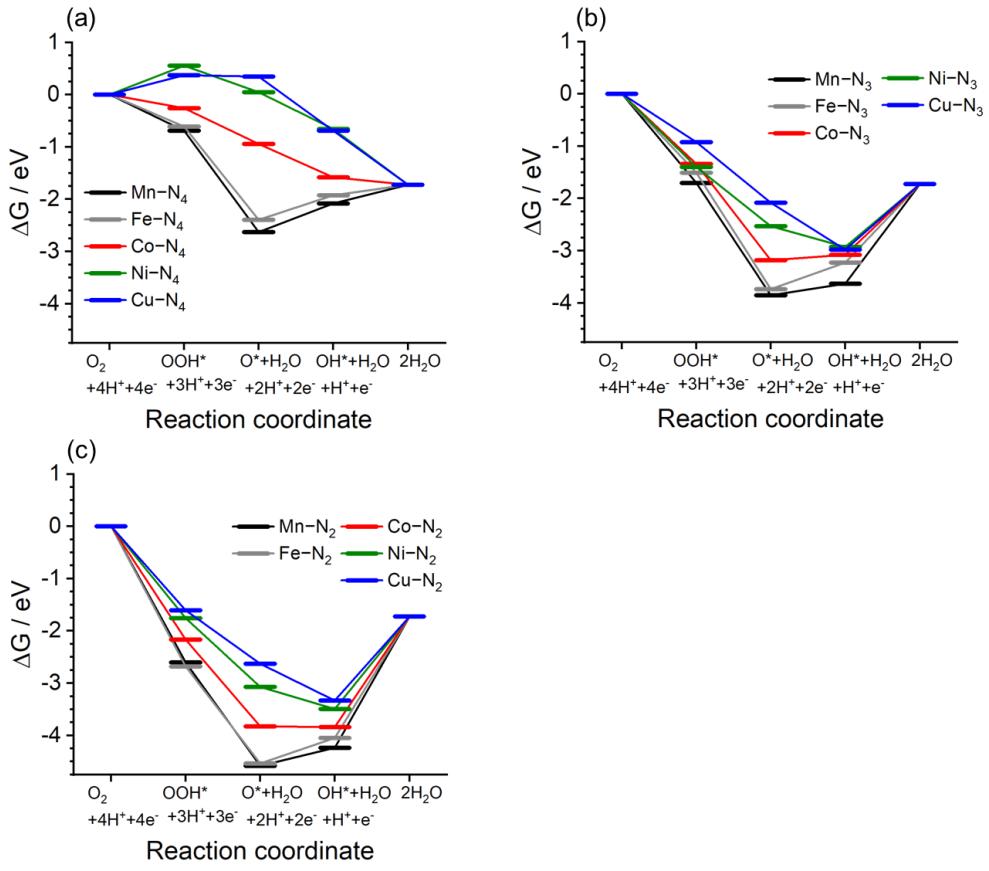

Figure S7. Free energy diagram for each reaction coordinate for ORR. (a) M−N_4, (b) M−N_3 and (c) M−N_2. Electrode potential = 0.8 V vs. CHE.

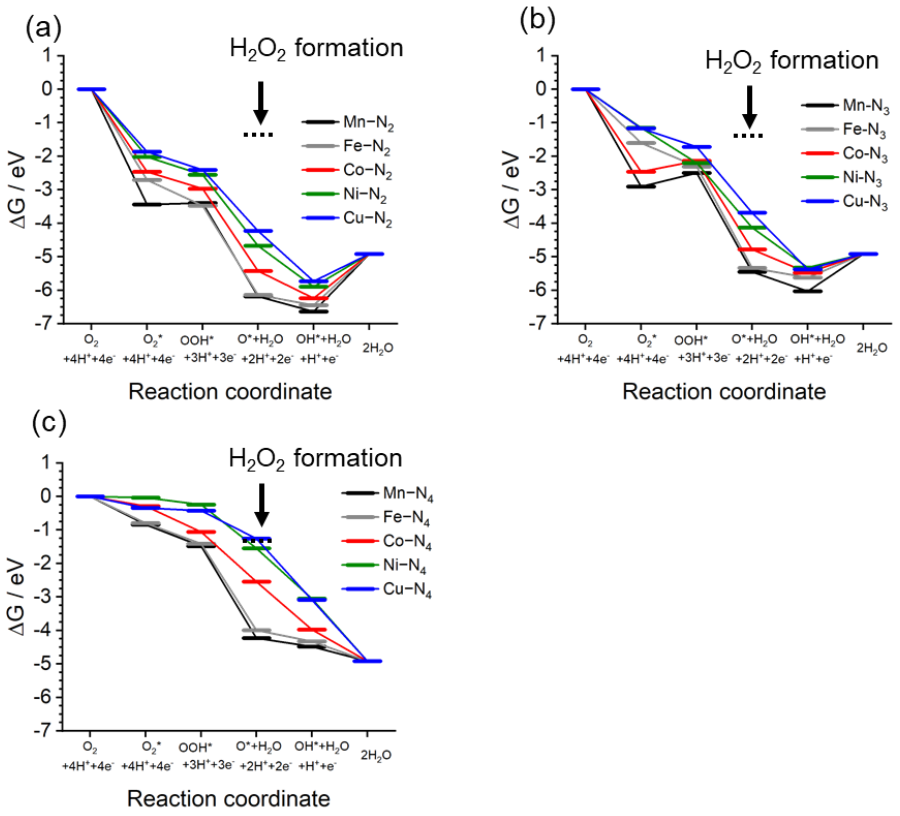

Figure S8. Free energy diagrams for each reaction coordinate for ORR including O_2 molecule adsorption steps and H_2O_2 formation steps. (a) M−N_2, (b) M−N_3 and (c) M−N_4. Electrode potential = 0 V vs. CHE.

Note: In these diagrams, the H_2O_2 formation energy is set to 1.36 eV (= 0.68×2). As shown in this figure, only Cu−N_4 and Ni−N_4 possibly catalyze H_2O_2 formation. Thus, the $4e^-$ process, H_2O formation is more favorable than $2e^-$ process (H_2O_2 formation) for most of M−COFs.

O_2 adsorption step was calculated to check whether the O_2 adsorption step affects a rate-determining step for ORR or not. First, the adsorption of O_2 molecule is exothermic for all M−COFs. In addition, for the M−COFs on the left-hand side of the volcano in Figure 6 (*i.e.* the H_2O formation from OH* is the rate determining), the energy barrier of the formation of OOH* from adsorbed O_2 was equal to or smaller than that of the H_2O formation from OH*. These results indicate that our conclusion about the rate-determining steps were not affected even when considering the O_2 adsorption.

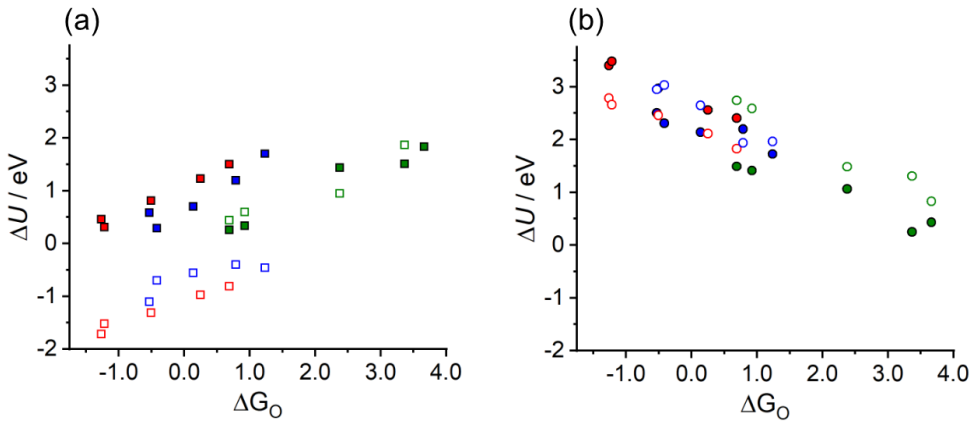

Figure S9. Potential plots for limiting steps of ORR against ΔG_O. (a) Desorption step for H_2O (open square) and OH* formation (closed square). (b) formation step of OOH* (closed circle) and O* formation (open circle). For both graphs, red: M−N_2, blue: M−N_3 and green: M−N_4.

Note: Basically, (a) OH* formation (closed square) is more positive than H_2O formation (open square) more than 2.35 eV and (b) O* formation (open circle) is more positive than OOH* formation (closed circle) less than 2.35 eV. This means that either H_2O formation or OOH* formation is limiting potential steps for ORR among M−COF catalysts as described in main manuscript. The limiting potential for OH* (ΔU_3) and O* (ΔU_4) is calculated as shown below.

$$\Delta U_3 = -(\Delta G_{OH} - \Delta G_O)$$
$$\Delta U_4 = -(\Delta G_O - \Delta G_{OOH})$$

Table S4 ΔE_{ads} of ORR intermediates calculated in this study.

(M-N_2)	**O**	**OH**	**OOH**
Mn	**-0.59**	**-1.70**	**1.57**
Fe	**-0.55**	**-1.51**	**1.49**
Co	**0.16**	**-1.30**	**2.00**
Ni	**0.92**	**-0.95**	**2.41**
Cu	**1.36**	**-0.79**	**2.57**

(M-N_3)	**O**	**OH**	**OOH**
Mn	**0.14**	**-1.09**	**2.47**
Fe	**0.25**	**-0.69**	**2.67**
Co	**0.81**	**-0.54**	**2.83**
Ni	**1.46**	**-0.39**	**2.78**
Cu	**1.90**	**-0.44**	**3.25**

(M-N_4)	**O**	**OH**	**OOH**
Mn	**1.36**	**0.45**	**3.48**
Fe	**1.59**	**0.61**	**3.56**
Co	**3.05**	**0.96**	**3.91**
Ni	**4.04**	**1.88**	**4.72**
Cu	**4.33**	**1.85**	**4.54**

Table S5 Collected data of solvation energies of ORR intermediates for molecular catalysts used in previous studies.

	Value	Material
O*	−0.7	This study
	0.23	BN[a]
	−0.15	Fe−Pc[b]
	−0.76	Cu/CTF[c]
	−0.53	N−C[d]
	-	M−Nx[e]
OH*	−0.38	This study
	−0.62	BN[a]
	−0.2	Fe−Pc[b]
	−0.61	Cu/CTF[c]
	−0.42	N−C[d]
	−0.3	M−Nx[e]
OOH*	−0.47	This study
	−1.18	BN[a]

Fe–Pc[b]	−0.17
Cu/CTF[c]	−0.38
N–C[d]	−0.49
M–Nx[e]	−0.3

a: Ref. 13, b: Ref. 14, c: Ref. 10, d: Ref. 15, e: Ref. 16

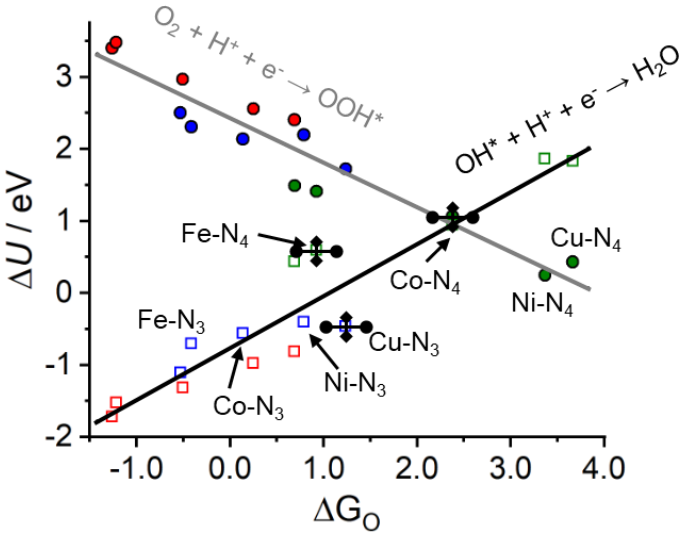

Figure S10. Replotted potential plots for the limiting steps of the ORR against the ΔG_{ads} values with error bars for Cu–N_3, Co–N_4 and Fe–N_4. Error bars represent the mean absolute errors of 5 or 6 values for

solvation energies of O*, OH* and OOH*.

References

(1) Calle-Vallejo, F.; Martinez, J. I.; Rossmeisl, J., Density functional studies of functionalized graphitic materials with late transition metals for oxygen reduction reactions. *Phys. Chem. Chem. Phys.* **2011,** *13* (34), 15639-15643.

(2) Calle-Vallejo, F.; Martínez, J. I.; García-Lastra, J. M.; Abad, E.; Koper, M. T. M., Oxygen reduction and evolution at single-metal active sites: Comparison between functionalized graphitic materials and protoporphyrins. *Surf. Sci.* **2013,** *607*, 47-53.

(3) Calle-Vallejo, F.; Tymoczko, J.; Colic, V.; Vu, Q. H.; Pohl, M. D.; Morgenstern, K.; Loffreda, D.; Sautet, P.; Schuhmann, W.; Bandarenka, A. S., Finding optimal surface sites on heterogeneous catalysts by counting nearest neighbors. *Science* **2015,** *350* (6257), 185-189.

(4) Nørskov, J. K.; Rossmeisl, J.; Logadottir, A.; Lindqvist, L.; Kitchin, J. R.; Bligaard, T.; Jónsson, H., Origin of the overpotential for oxygen reduction at a fuel-cell cathode. *J. Phys. Chem. B* **2004,** *108* (46), 17886-17892.

(5) Kattel, S.; Atanassov, P.; Kiefer, B., Catalytic activity of Co-N(x)/C electrocatalysts for oxygen reduction reaction: a density functional theory study. *Phys. Chem. Chem. Phys.* **2013,** *15* (1), 148-153.

(6) Sha, Y.; Yu, T. H.; Liu, Y.; Merinov, B. V.; Goddard, W. A., Theoretical study of solvent effects on the platinum-catalyzed oxygen reduction reaction. *J. Phys. Chem. Lett.* **2010,** *1* (5), 856-861.

(7) Kattel, S.; Atanassov, P.; Kiefer, B., Density functional theory study of Ni–Nx/C electrocatalyst for oxygen reduction in alkaline and acidic media. *J. Phys. Chem. C* **2012,** *116* (33), 17378-17383.

(8) Zheng, Y.; Jiao, Y.; Zhu, Y.; Cai, Q.; Vasileff, A.; Li, L. H.; Han, Y.; Chen, Y.; Qiao, S. Z., Molecule-level g-C3N4 coordinated transition metals as a new class of electrocatalysts for oxygen electrode reactions. *J. Am. Chem. Soc.* **2017,** *139* (9), 3336-3339.

(9) Cui, X.; An, W.; Liu, X.; Wang, H.; Men, Y.; Wang, J., C_2N-graphene supported single-atom catalysts for CO_2 electrochemical reduction reaction: mechanistic insight and catalyst screening. *Nanoscale* **2018,** *10* (32), 15262-15272.

(10) Patel, A. M.; Ringe, S.; Siahrostami, S.; Bajdich, M.; Nørskov, J. K.; Kulkarni, A. R., Theoretical approaches to describing the oxygen reduction reaction activity of single-atom catalysts.

J. Phys. Chem. C **2018,** *122* (51), 29307-29318.

(11) Aiyappa, H. B.; Thote, J.; Shinde, D. B.; Banerjee, R.; Kurungot, S., Cobalt-modified covalent organic framework as a robust water oxidation electrocatalyst. *Chem. Mater*. **2016**, 28 (12), 4375-4379.

(12) Lin, S.; Diercks, C. S.; Zhang, Y. B.; Kornienko, N.; Nichols, E. M.; Zhao, Y.; Paris, A. R.; Kim, D.; Yang, P.; Yaghi, O. M.; Chang, C. J., Covalent organic frameworks comprising cobalt porphyrins for catalytic CO_2 reduction in water. *Science* **2015**, 349 (6253), 1208-1213.

(13) Lyalin, A.; Nakayama, A.; Uosaki, K.; Taketsugu, T., Theoretical predictions for hexagonal BN based nanomaterials as electrocatalysts for the oxygen reduction reaction. *Phys. Chem. Chem. Phys*. **2013**, 15 (8), 2809-2820.

(14) Mussell, S.; Choudhury, P., Density functional theory study of iron phthalocyanine porous layer deposited on graphene substrate: A Pt-free electrocatalyst for hydrogen fuel cells. *J. Phys. Chem. C* **2016**, 120 (10), 5384-5391.

(15) Yu, L.; Pan, X.; Cao, X.; Hu, P.; Bao, X., Oxygen reduction reaction mechanism on nitrogen-doped graphene: A density functional theory study. *J. Catal*. **2011**, 282 (1), 183-190.

(16) Chan, Y.-T.; Tsai, M.-K., The role of metal-oxo intermediate to oxygen reduction reaction catalysis: A theoretical investigation using nitrogen-substituted carbon nanotube models. *Surf. Sci*. **2018**, 677, 301-305.